Modelling the soiling rate: Dependencies on meteorological parameters

Cite as: AIP Conference Proceedings **2126**, 190018 (2019); https://doi.org/10.1063/1.5117715
Published Online: 26 July 2019

Fabian Wolfertstetter, Stefan Wilbert, Felix Terhag, et al.

Modelling the Soiling Rate: Dependencies on Meteorological Parameters

Fabian Wolfertstetter[1, a)], Stefan Wilbert[1], Felix Terhag[1, 2], Natalie Hanrieder[1], Aranzazu Fernandez-García[3], Christopher Sansom[4], Peter King[4], Luis Zarzalejo[5], Abdellatif Ghennioui[6]

[1]*German Aerospace Center (DLR), Ctra de Senés km4, 04200 Tabernas, Spain*
[2]*Mathematical Institute of the University of Cologne, Weyertal 86-90, 50931 Cologne, Germany*
[3]*CIEMAT, Plataforma Solar de Almería, Ctra. de Senés km 4, 04200 Tabernas, Spain*
[4]*Cranfield University, Building 90, Cranfield, Bedfordshire, UK*
[5]*CIEMAT, Renewable energy department, Avda. Complutense, 40, Madrid, Spain*
[6]*IRESEN, Green Energy Park Benguerir, Morocco*

[a)]Corresponding author: Fabian.wolfertstetter@dlr.de

Abstract. Concentrating solar power (CSP) plants are often located in dusty environments. Soiling depends strongly on location, time, weather conditions and mirror orientation and is characterized by the soiling rate: the loss of the specular reflectance due to soiling per time interval. The average soiling rate can reach 2%/day on sites with heavy dust loads such as the Arabian Peninsula. On some days (for example during a sandstorm) the soiling rate can be significantly higher than that. Measurement campaigns for the soiling rate are of interest for the CSP plant site selection and the plant design, but they are time consuming and costly. In this study, a soiling model is presented that describes particle deposition processes based on physical equations from where the soiling rate can be derived. The model uses easily measureable meteorological parameters such as aerosol particle number concentration, wind speed and direction at 10 m height, relative humidity, temperature and precipitation as input parameters. The model has been optimized and validated using measurement data from two sites in Morocco and Spain. The measurement data have been divided into two parts. One was used to find optimum model parameters by parameterization. The second dataset was used to validate the model. The model reaches a bias of 0.1%/d and a root mean square deviation of 0.4 %/d. Days with weak soiling (<1%/d) rates are identified with an accuracy of more than 90 %, the question whether or not the soiling rate is above 1%/d is answered correctly in 85 % of the cases.

INTRODUCTION

Concentrating solar power (CSP) plants are being implemented in dusty environments such as the Middle East and North Africa (MENA) regions. The trade-off between minimizing soiling-induced losses and cleaning costs is a challenge for operators and project planners. Measurement campaigns for the quantification of soiling of CSP on future or existing sites are time consuming and costly(Suellen C.S. Costa, 2016).

There exist only few studies that correlate the soiling rate of concentrating solar collectors to other weather parameters. Tahboub et al. showed that there is no clear linear relation to the irradiance components, the relative humidity, wind or temperature for a site in Abu Dhabi (Tahboub, Dahleh, & Goebel, 2011). A study performed in southern Portugal confirmed these findings, investigating also aerosol particle mass concentration. They also applied neural network approaches to predict soiling rates (Conceição, Silva, & Collares-Pereira, 2018). A NREL study could correlate the annual mean PM10 (particulate matter per volume of air up to a particle diameter of 10 µm) value of PV power plant sites to the annual mean soiling rate of the installation (Micheli & Muller, 2017).

The present study aims at increasing the understanding of soiling mechanisms such as particle and dust adhesion to surfaces and develop a soiling model that derives the soiling rate from other weather data. This understanding

SolarPACES 2018
AIP Conf. Proc. 2126, 190018-1–190018-11; https://doi.org/10.1063/1.5117715
Published by AIP Publishing. 978-0-7354-1866-0/$30.00

enables an estimation of the soiling rate from more broadly available weather data such as aerosol particle concentration, wind, relative humidity and others. The soiling model is developed based on the physical principles implemented in existing atmospheric dust transport models. These are applied to the soiling of a CSP solar field.

The availability of time resolved soiling rate data enables the development of advanced cleaning strategies and an improvement of site selection, the yield analysis and resource assessment procedures (F. Wolfertstetter, Wilbert, S., Dersch, J., Dieckmann, S., Pitz-Paal, R., & Ghennioui, A, 2018).

MEASUREMENT SITES AND INSTRUMENTS

The two measurement sites for the soiling model development used in this study are Missour, Morocco at latitude 32.86 °N and longitude 4.11 °W and CIEMAT‘s Plataforma Solar de Almeria (PSA), Spain at latitude 37.09 °N and longitude 2.35 °W. Pictures of the measurement site of Missour, Morocco and PSA are shown in FIGURE 1. Both sites are equipped with the instruments described in the following section. Both sites are classified as arid according to the Köppen-Geiger climate classification map (Kottek, Grieser, Beck, Rudolf, & Rubel, 2006).

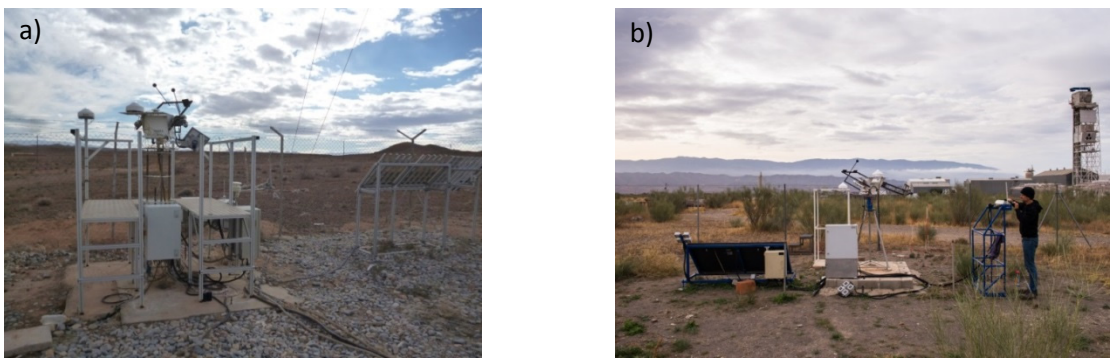

FIGURE 1. Measurement sites in a) Missour, Morocco and b) CIEMAT’s Plataforma Solar de Almería, Spain.

Soiling Rate Reference Measurement

The Tracking Cleanliness Sensor (TraCS) is used as a reference in this study. It has been described in (F. Wolfertstetter, 2013, 2016; F. Wolfertstetter, K. Pottler, N. Geuder, R. Affolter, A. A. Merrouni, A. Mezrhab, and R. Pitz-Paal, 2014). The soiling rate measured between 2014 and 2017 at PSA is shown in FIGURE 2. There are 16 days showing a high soiling rate stronger than -3% /day. The average soiling rate in that time period is -0.52% /day with a standard deviation of 0.2% /day (absolute standard deviation). The mirror of the TraCS system follows the suns movement throughout the course of a day with a 15° offset that is caused by the 15° incidence angle used in the cleanliness measurement. After sunset, the tracker parks the mirror in a vertical position facing 105° N until sunrise. The mirror’s orientation is thus at least similar to that of a parabolic trough or a heliostat, because the latter also describe a movement relative to the sun during the day and are parked in a near-vertical position at nights, depending on the type of collector or heliostat. The measurements are taken at a height of approximately 1.5 m above ground at both sites. Both TraCS instruments are located at a fairly open terrain with little objects to block air streams from hitting the sample mirror’s surface.

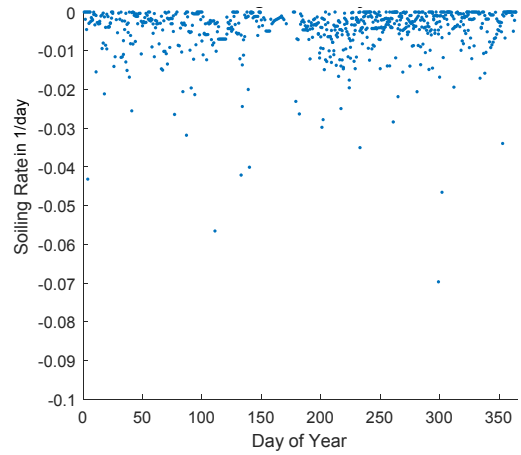

FIGURE 2. Soiling rate dataset in daily time resolution as measured at PSA between 2014 and 2017. Data measured in different years is overlayed.

Weather Parameter Measurements

For measurement of the aerosol particle size distribution, the EDM164 of Grimm GmbH is used. It is an optical particle counter (OPC) that determines the particle size distribution function per volume of air by a scattering measurement. The instrument aspires air into a nozzle inlet located on the instrument body. The air stream passes a measurement chamber that is passed by a laser beam. A laser diode of 655 nm illuminates a defined measurement volume where each particle passes through. The scattered signal is collected at an angle of 90° by a reflecting mirror with an aperture angle of 30° and is reflected by the mirror into a photo diode detector. A light trap avoids strong noise effects. The amount of reflected laser light is then proportional to the particle size. The counting rate can be derived from the reflected light amount and the flow rate.

To derive the particle size from the reflected light intensity, an assumption about the scattering phase function has to be made. This is included in the internal EDM164 post-processing software. Also an assumption about the particle shape has to be made. For simplicity reasons, a spherical shape of the particles is assumed.

The instrument registers a passing particle by detecting a stray light pulse in its detectors. It derives the particle size from the amplitude of each of the signals. The resulting counts of particles are saved in a resolution of 31 size channels ranging from 0.25 to 31 µm. The wind speed is measured by rotating cup anemometers and wind vanes mounted at 10 m height above ground.

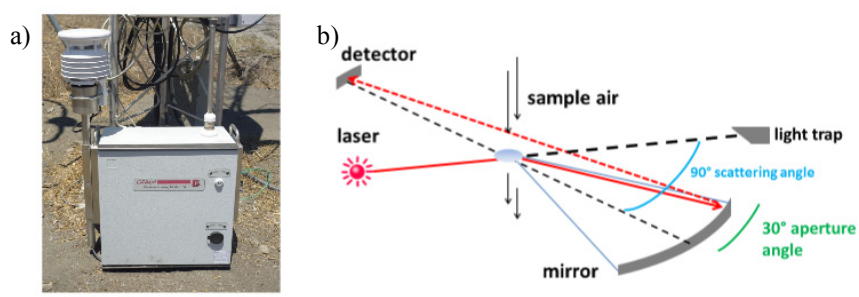

FIGURE 3. a) The Grimm EDM164 instrument to measure the particle number size distribution function at PSA, b) Sketch of the measurement chamber of the EDM 164 instrument following (Grimm, 2009)

The measurements described here are used for the development and validation of the soiling model described below. They serve as the framework for the possible model variables that can be used. Furthermore the datasets are divided into two sets: The training dataset is used to better determine model parameters by parameterization and the validation set is used to quantify the model quality.

SOILING MODEL DEVELOPMENT

The CSP soiling model developed in this work is based on existing models for the dry deposition of dust over geographic regions. The final equations have been designed according to the available meteorological measurements and to the problem of dust deposition on a mirror surface in a solar field. These measurement parameters have been chosen such that physically motivated equations can be elaborated and tested with actual measurement data.

Model Structure

The here presented model describes the deposition of particles on a mirror surface from its surroundings. Atmospheric dust transport models (ADTM) such as the NMMB-MONARCH (Badia et al., 2017) by Barcelona Supercomputing Center or the NASA GEOS-5 (Reichle, De Lannoy, Forman, Draper, & Liu, 2014) determine the average particle mass in 3 to 8 size classes deposited in an area with a spatial resolution of 1 to 5 kilometers, depending on the model and the latitude. The equations from the ADTMs can therefore not be applied directly to the problem of mirror soiling. However, studies in this area of research can be transferred to some degree. In ADTMs, the particle deposition from the atmosphere on the ground is described as a flux F of particles in the direction of the earth's surface – and in application to CSP reflectors towards the mirror surface - according to

$$F_{mirr}(d_p) = v_D(d_p) \cdot C(d_p), \tag{1}$$

with the particle concentration C and the deposition velocity v_D, both given in dependence of the particle diameter d_p. The particle flux describes the number of particles which settle on an area per time interval. v_D is given in units of m/s and is the parameter that is determined by a model of the physical processes. $C(d_p)$ is given in units of 1/m³ and can be taken directly from the optical particle counter measurements for our soiling model.

In ADTMs a distinction is made between dry and wet particle deposition. Wet deposition refers to water-induced deposition. CSP technology is usually implemented in arid regions such that wet deposition does not occur frequently. Nevertheless, even at such sites there are events when very light rainfall coincides with high atmospheric aerosol concentration levels that lead to the so-called "red rain" events where particles are washed out of the atmosphere and deposited. Red rains are the only significant contribution to solar mirror soiling from the wet deposition regime. Based on observations and soiling rate measurements, at PSA 3 to 6 red rain events are detected each year. They are added to the model separately by a correlation between rain amount and soiling rate derived from the PSA measurement data.

The equation system for the dry deposition in ADTMs is based on the analogy with an arrangement of resistances. In this image frame, airborne particles have to overcome resistances when moving towards the earth's surface. The aerodynamic resistance R_a quantifies the air's resistance to moving objects. The surface resistance R_s describes the resistance during interaction of a surface and the boundary air layer. The gravitational settling velocity of the particles is represented by v_S. Therefore, the dry deposition can be described as

$$v_D = v_S + \frac{1}{R_a + R_s}. \tag{2}$$

The aerodynamic resistance R_a can be neglected here because the particle concentration is being measured at the point of interest in our case, i.e. close to the mirror surface. When modelling the remaining Rs, the following processes have to be taken into account: impaction, interception, Brownian motion and sedimentation. The deposition velocity of the particles is the sum of the deposition velocities of the different deposition mechanisms. Therefore, equation (2) can be written as

$$v_D = v_S + \frac{1}{R_s} = v_S + v_B + v_{In} + v_{Im}. = v_S + u_*(E_B + E_{IN} + E_{IM}) \cdot K_1. \tag{3}$$

The terms in the brackets represent the rate of deposition of the Brownian motion (E_B), interception (E_{IN}) and impaction (E_{IM}) that will be described in more detail below. Rebound of particles is represented by the parameter K_1 that is dependent on the wind velocity, surface humidity and relative humidity.

The wind friction velocity u_* describes the logarithmic wind profile as commonly assumed in literature:

$$u_* = u_{Wind} \cdot \frac{\kappa}{\ln\left(\frac{z_R}{z_0}\right)}, \tag{4}$$

Where ZR is the height above ground and Z0 is the surface roughness length. κ is the Von Karman constant that is widely agreed to have a unitless value of 0.4 (Frenzen & Vogel, 1995). Because ZR is the height of the mirror above ground, the wind friction velocity is directly proportional to the wind velocity in this model.

Particle Deposition Mechanisms

In what follows, the different deposition processes are described in detail and each of them is assigned a global weighting factor to account for the different influence on the particle deposition. These weights are determined by a parameterization based on measurement data.

Sedimentation

Sedimentation or also called "gravitational settling" describes the settling of aerosol particles towards the ground due to gravity. The deposition velocity is described by Stoke's Law. It is valid for flows with a low Reynold's number and laminar flow. It is derived from the equilibrium of friction, buoyant and gravitational forces. The deposition velocity of a particle in air due to gravity is

$$v_{S,p} = \frac{g \cdot {d_p}^2 (\rho_{aero} - \rho_{air})}{18\, \eta_{air}}, \tag{5}$$

Where g is Newton's gravitational constant, d_p is the diameter of the aerosol particle, ρ_{aero} refers to the particles material density, which is assumed as constant: $\rho_{aero} = 2650\ \mathrm{kg/m^3}$ this value has been taken from (Wagner et al., 2009) and is the average over the densities from four different sampling campaigns. For simplicity and as their variation has a much smaller influence than other assumptions, the properties of the air are assumed as constant in the following and are taken for standard conditions.

For the problem of soiling, only those particles are considered that end up on the optical surface of a solar collector. Collector surfaces are generally not horizontally mounted and are being moved throughout the day to track the sun. Equation (5) accounts for particles that deposit on a horizontal surface. It must be adapted to the inclined surface, because, the particle flux perpendicular to the mirror surface has to be calculated, and therefore the particle deposition velocity perpendicular to the reflector surface, v_S, is calculated as

$$v_S = \cos(\alpha_{el}) \cdot v_{S,p} = \cos(\alpha_{el}) \cdot \frac{g \cdot {d_p}^2 (\rho_{aero} - \rho_{air})}{18\, \eta_{air}}, \tag{6}$$

where α_{el} is the elevation angle of the reflector surface. The angle definition is illustrated in FIGURE 4

The deposition velocity by gravity is dominated by the particle size and the elevation angle of the mirror. The latter can be confirmed by the lower soiling rates detected on vertically exposed mirrors in the literature compared to upward facing mirrors. Equation (6) results in a gravitational deposition velocity in units of m/s towards the mirror surface.

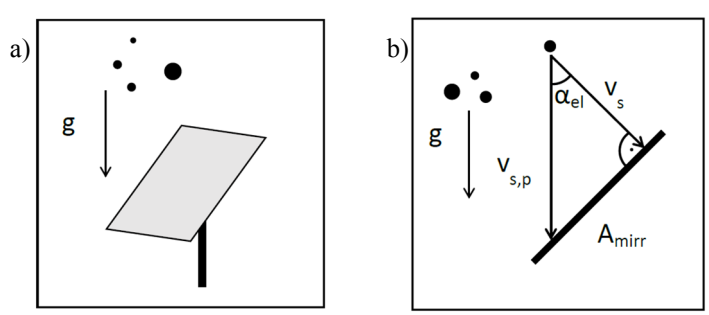

FIGURE 4. a) Illustration of the gravitational deposition mechanism and b) the parameter definitions.

Brownian Motion

Soil particles are put into motion by random impacts from surrounding air molecules and other aerosol particles that move in function of the temperature of the surrounding medium. This random movement is called Brownian motion and is interpreted as a diffusion process. The transport of particles can be described following the Einstein Smoluchowski relation with the diffusion coefficient D_B that can be calculated from the temperature and viscosity of the air surrounding the solar mirror and the particle diameter. The relation holds for low Reynolds numbers and non-turbulent flows. Next, the Schmidt number is introduced that is the ratio of motion caused by diffusion processes and those caused by impaction. The Schmidt number is calculated as

$$S_C = \frac{\nu_{air}}{D_B}. \tag{7}$$

ν_{air} is the kinematic viscosity. A low Schmidt number indicates that diffusion constitutes the main contribution for transport processes. In deriving the deposition velocity for Brownian motion we will follow the line of arguments given in reference (Slinn, 1982). There it is assumed that the Schmidt number is directly proportional to the wind speed.

The Parameter a_{brown} will quantify the relative contribution of the Brownian motion to the total deposition velocity in comparison to the other deposition mechanisms. The resulting equation for the deposition velocity due to Brownian motion is

$$\begin{aligned} v_B &= a_{brown} \cdot u_{wind} \cdot {S_C}^{-0.667} = a_{brown} \cdot u_{wind} \left(\frac{\nu_{air}}{D_B}\right)^{-0.667} \\ &= a_{brown} \cdot u_{wind} \cdot \left(\frac{\nu_{air} \cdot 3 \cdot \pi \cdot \eta_{air} \cdot d_p}{k_B \cdot T_{air}}\right)^{-0.667}, \end{aligned} \tag{8}$$

where T_{air} is the air temperature and η_{air} the dynamic viscosity of the air.

Impaction

Air molecules move not only randomly by temperature fluctuation but can also follow an air flow. In outdoor conditions, an air flow is characterized by the measurement of wind speed and direction. If the flow hits an obstacle like a solar mirror, the stream lines are being deviated from its original path. An example of such a deviation is shown schematically in FIGURE 5.

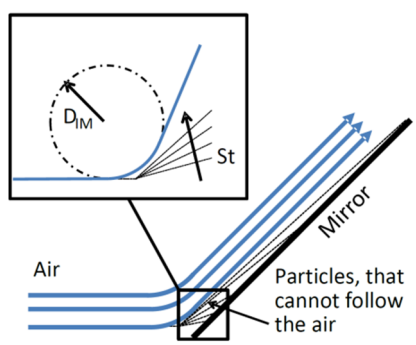

FIGURE 5. Illustration for the mechanism of particle impaction on a mirror surface

The radius of curvature D_{IM} is the leading parameter to determine the strength of direction change. The Stokes number quantifies the potential of particles to follow an air stream. It is a dimensionless parameter. It is defined as the ratio between the time it takes for a particle to adapt to changes in an air flow by friction with the medium's molecules and the time it takes the medium itself to change its flow speed or direction. For small Reynold's numbers, i.e. laminar flow profiles, the Stokes number can be written as

$$St = \frac{\rho_{aero}}{18\,\eta_{air}} \cdot {d_p}^2 \cdot \left(\frac{u_{wind}}{D_{Im}}\right). \tag{9}$$

The flow deviation is dependent on the orientation of the mirror relative to the air flow direction (wind direction). Particles with high Stokes numbers cannot follow the air flow, while those with $\mathrm{St} < 1$ remain suspended in air and do not impact on the obstacle. In order to represent that in terms of deposition efficiency E_{Im}, we chose to follow (Muyshondt, Anand, & McFarland, 1996) assuming a sigmoidal distribution of the deposition efficiency:

$$E_{Im} = \mathrm{Sig}(\mathrm{St}) = \frac{1}{1 + \exp(-f_{Im}(\mathrm{St} - 1))}. \tag{10}$$

This function assumes 0 for $\mathrm{St} \ll 1$ and 1 for $\mathrm{St} \gg 1$. The parameter f_{Im} determines how steeply $\mathrm{Sig}(\mathrm{St})$ transitions between 0 and 1. For St equal to one $\mathrm{Sig}(\mathrm{St})$ assumes 0.5. f_{Im} will be determined during the parameterization based upon measurement data.

If a wind field hits a solar mirror with high velocity, the number of particles that pass by or hit the mirror per unit time increases proportionally to the wind speed. Therefore, $\mathrm{Sig}(\mathrm{St})$ is multiplied with the wind speed. Only the component of the wind vector that points perpendicular towards the optical mirror surface should be taken into account. It is quantified by the parameter σ_{or}. The resulting deposition velocity caused by impaction can be written as

$$v_{Im} = a_{Im} \frac{\sigma_{or} \cdot u_{Wind}}{1 + \exp(-f_{Im}(\mathrm{St} - 1))}. \tag{11}$$

Again, the factor a_{Im} serves as a weighting factor between the different deposition mechanisms. For higher wind speeds smaller particles can deposit onto the mirror surface and they show higher deposition velocities due to the higher wind speed.

σ_{or} is a factor to the wind speed that returns $v_{\perp}$, the component of the wind velocity hitting the mirror's front side perpendicularly as in

$$v_{\perp} = \sigma_{or} \cdot u_{Wind} \tag{12}$$

Any vertical component of the wind speed is neglected. The difference between the azimuth wind direction and mirror azimuth orientation $\Delta\theta$ and the elevation angle of the mirror α_{el} are used to calculate σ_{or} following:

$$\sigma_{or} = \begin{cases} 0 & , \quad \text{for } \cos(\Delta\theta) \cdot \sin(\alpha_{el}) \leq 0 \\ \cos(\Delta\theta) \cdot \sin(\alpha_{el}), & \text{for } \cos(\Delta\theta) \cdot \sin(\alpha_{el}) \geq 0 \end{cases}. \tag{13}$$

The mirror orientation towards the wind direction not only influences the mass flux hitting the mirror, but also the curvature of the air flow at the mirror. This curvature influences the Stokes number and is quantified by the radius of curvature D_{Im}. The latter is inversely dependent on σ_{or} according to

$$D_{Im} = \frac{d_{Im}}{\sigma_{or}}. \tag{14}$$

For $\sigma_{or} = 1$ the wind flow hits the mirror surface perpendicular and is deviated strongly with a small curvature radius. d_{Im} is a factor of proportionality and a model parameter that will be determined in the parameterization.

Summary of the Model Equations

The deposition velocity results from the addition of the deposition velocities caused by the mechanisms of sedimentation, Brownian motion and impaction that have been described above.

$$v_D = v_S + v_B + v_{Im} \tag{15}$$

The process of particle deposition depends on the environmental conditions that are reflected in the model variables. The model variables are meteorological measurement parameters and the mirror orientation of the sample mirror. For the validation of the model we use the orientation of the TraCS measurement system's mirror. The model parameters on the other hand describe the quality and proportionality of certain processes. They are determined once in a parameterization using a training measurement data set and are set as constants from there on. The particle diameter is the most influential model variable that appears in all three deposition mechanisms. The wind speed has an influence on Brownian motion and impaction.

In the example shown in FIGURE 6, the deposition velocity is shown in dependency of the particle diameter. The wind hits the mirror that is tilted by 45° centrally which results in $\sigma_{or} = 0.7$. Going to higher wind speeds, smaller particles are affected by impaction. The form of the curves in FIGURE 6 reflects the influences of the different particle deposition processes. At zero wind conditions, only sedimentation occurs and deposition velocity

is reduced to equation (6)(6). Going to higher wind speeds, the impaction, rebound and Brownian motion terms gain more influence on the particle deposition.

"Rebound" is the process of particles bouncing off the mirror surface after they came into contact with it. It depends on the particles kinetic energy, the relative humidity and a model parameter. The effect is not described in detail here due to space limitations. It can be seen in FIGURE 6 that it increases with higher wind speeds and affects smaller particles when the wind is stronger.

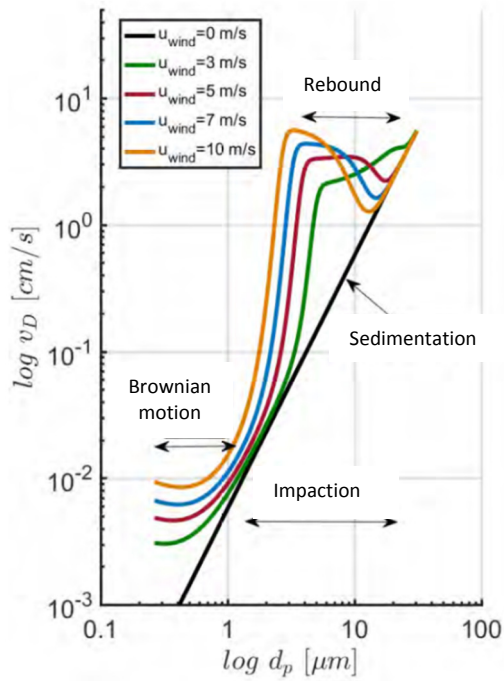

FIGURE 6. Deposition velocity against the particle diameter for different wind speeds and laminar air flow conditions.

Rate of Surface Coverage

Once the particle deposition velocity and aerosol particle number concentration in the surrounding air volume are known, the rate of particles attaching to the mirror surface can be calculated, according to equation (1). For application to CSP, the parameter of interest is not the number of particles attached to the mirror, but the optical loss caused by these particles. To this end, the projected surface covered by a certain particle number with a given size distribution attached to the mirror surface is derived. The mirror area covered by a particle is defined as the shadowed area on the mirror plane if the light would impinge perpendicular on the mirror.

Assuming a deposition Flux Fmirr corresponding to a particle number concentration C of spherical particles in the surrounding air that deposit with the deposition velocity v_D on a mirror surface, the rate of surface coverage CR can be written as

$$CR = \sum_{d_p=0.25\mu m}^{32\mu m} F_{mirr}(d_p) \cdot {d_p}^2 \cdot \frac{\pi}{4} = \sum_{d_p=0.25\mu m}^{32\mu m} v_D(d_p) \cdot C(d_p) \cdot {d_p}^2 \cdot \frac{\pi}{4} \tag{16}$$

CR describes which fraction of the mirror surface is covered by particles per time interval. Therefore, we can assume that CR is proportional to the soiling rate. The slope of the connecting linear equation is negative. This proportionality holds for particles of same size and composition. If the latter parameters are subject to change which is the case for naturally occurring particles, the assumption is to be proven true. The change of the reflectance with the incidence angle as described in (Heimsath et al., 2016) for the application of the soiling data to CSP plants can be modelled in a separate software module. For the validation of the model with TraCS data that is presented here a constant incidence angle is used so that we do not have to consider such its variation in this work. More details on

the model and its performance can be found in the project report of the European WASCOP project (F. Wolfertstetter, Wilbert, Fernández-García, & Azpitarte, 2018).

RESULTS AND DISCUSSION

The complete PSA dataset described in in the measurement section above is used for the development of the model. Four fifth of the dataset are used to fit the calculated model output to the measurement of the soiling rate. K-fold validation (Picard & Cook, 1984) has been applied in the development and validation of the model. Its purpose is to increase the statistical significance of the evaluation and to limit errors caused by coincidence. It can avoid an underestimation of the model quality if the test dataset covers a parameter and/or sample space that differs from that covered by the training data set.

As the goodness of fit, the root mean squared error (RMSE) is used. In practice, the model parameters are varied on a grid and the model is evaluated on the training dataset, compared to the measured soiling rate and assigned a RMSE. Once this procedure has been repeated for the complete grid of parameter values, the set of parameter values with the lowest RMSE can be selected. The model parameters are then used to calculate the soiling rate from the validation weather data set. The result is compared to the measurement of the soiling rate for the same days to qualify the performance of the model.

FIGURE 7 shows the comparison of the modelled soiling rate (SR) to the measured soiling rate for the validation data sets from PSA and Missour. The model parameters used to evaluate the model at both sites are those determined on the PSA training set. The overall impression of the two scatterplots is similar. The scatter in the data is comparable; the slopes of imaginary linear fits to the data differ noticeable. There are less data points in the PSA validation set, because only one fifth of the data is shown there. The rest is used in the parameterization.

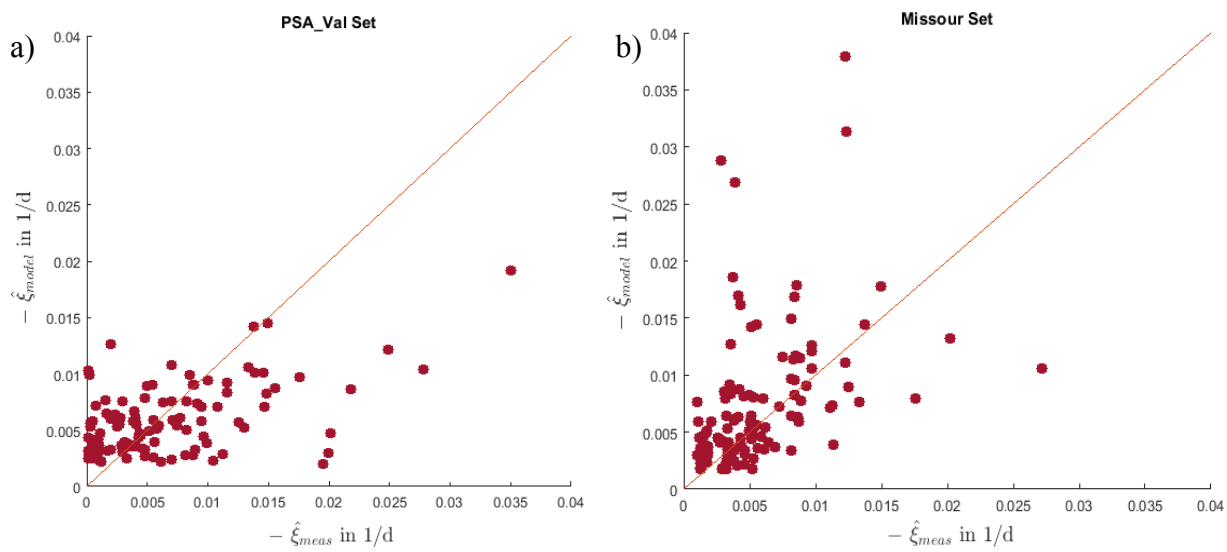

FIGURE 7: Scatter plots comparing the calculated and the measured soiling rate for the validation data sets from two sites. The parameterization has been performed on 80 % of the PSA dataset and has been validated for Missour without modification of the parameters.

The statistical parameters used to quantify the model quality are shown in TABLE 1. The bias is low compared to the measurement accuracy of the reference soiling rate measurement device. The average soiling rate for PSA is 0.5 %/d and the measurement accuracy of the TraCS reference instrument is 0.2 %/d. Compared to these values, the RMSE of the model is low enough to predict the soiling rate with a sufficient reliability. The low bias makes predictions on average soiling loads sufficiently reliable for inter-site comparisons. The RMSE does not differ substantially between the two sites. This indicates that the physical behavior of particles is similar at both sites. This leads to the assumption that there are no different particle chemistries or particle deposition mechanisms present at both sites. More work would be needed to test that assumption to more regions of the world.

TABLE 1. Soiling model performance for the different data sets.

Dataset	Bias (%/d)	RMSE (%/d)
PSA training set	0.08	0.43
PSA validation set	0.11	0.44
Missour set	0.09	0.46

CONCLUSION

A soiling model based on physical deposition mechanisms has been developed and tested on measurement data. The model equations are taken from existing atmospheric dust transport models and have been applied to the problem of solar collector soiling. A test data set taken at Plataforma Solar de Almeria is used to fit the model parameters. A separate validation data set from two sites is used to quantify the model performance.

The model predicts the soiling rate with an RMSE of 0.44 %/day at the training site and 0.46 %/day for the second measurement site. The biases are 0.11 and 0.09 %/day. It can give a valuable estimation of the soiling conditions of a site in the absence of direct measurements of the soiling rate. This information can be applied to improve the the yield estimation of solar power plant projects.

The model has the potential to be integrated into atmospheric dust transport models in the future. A unified model could deliver global soiling rate forecasts and soiling maps.

ACKNOWLEDGMENTS

This project has received funding from the European Union's Horizon 2020 research and innovation program under grant agreement No. 654479 (WASCOP). We thank the Helmholtz Association and the European Commission for partly funding this work within the Helmholtz NREL Solar Energy Initiative (HNSEI).

REFERENCES

1. Badia, A., Jorba, O., Voulgarakis, A., Dabdub, D., García-Pando, C. P., Hilboll, A.,Janjic, Z. (2017). Description and evaluation of the Multiscale Online Nonhydrostatic AtmospheRe CHemistry model (NMMB-MONARCH) version 1.0: gas-phase chemistry at global scale. *Geoscientific Model Development, 10*(2), 609.
2. Conceição, R., Silva, H. G., & Collares-Pereira, M. (2018). CSP mirror soiling characterization and modeling. *Solar Energy Materials and Solar Cells, 185*, 233-239. doi: https://doi.org/10.1016/j.solmat.2018.05.035
3. Frenzen, P., & Vogel, C. A. (1995). On the magnitude and apparent range of variation of the von Karman constant in the atmospheric surface layer. [journal article]. *Boundary-Layer Meteorology, 72*(4), 371-392. doi: 10.1007/bf00709000
4. Grimm, H., Eatough, D.J. (2009). Aerosol Measurement: The Use of Optical Light Scattering for the Determination of Particulate Size Distribution, and Particulate Mass, Including the Semi-Volatile Fraction. *Journal of the Air & Waste Management Association*, 101-107.
5. Heimsath, A., Lindner, P., Klimm, E., Schmid, T., Moreno, K. O., Elon, Y., Nitz, P. (2016). *Specular reflectance of soiled glass mirrors–Study on the impact of incidence angles.* Paper presented at the AIP Conference Proceedings.
6. Kottek, M., Grieser, J., Beck, C., Rudolf, B., & Rubel, F. (2006). World Map of the Köppen-Geiger climate classification updated. *Meteorologische Zeitschrift, 15*(3), 259-263. doi: 10.1127/0941-2948/2006/0130
7. Micheli, L., & Muller, M. (2017). An investigation of the key parameters for predicting PV soiling losses. *Progress in Photovoltaics: Research and Applications, 25*(4), 291-307.
8. Muyshondt, A., Anand, N., & McFarland, A. R. (1996). Turbulent deposition of aerosol particles in large transport tubes. *Aerosol Science and Technology, 24*(2), 107-116.
9. Picard, R. R., & Cook, R. D. (1984). Cross-validation of regression models. *Journal of the American Statistical Association, 79*(387), 575-583.
10. Reichle, R. H., De Lannoy, G. J. M., Forman, B. A., Draper, C. S., & Liu, Q. (2014). Connecting Satellite Observations with Water Cycle Variables Through Land Data Assimilation: Examples Using the NASA GEOS-5 LDAS. [journal article]. *Surveys in Geophysics, 35*(3), 577-606. doi: 10.1007/s10712-013-9220-8
11. Slinn, W. G. N. (1982). Predictions for particle deposition to vegetative canopies. *Atmospheric Environment (1967), 16*(7), 1785-1794. doi: https://doi.org/10.1016/0004-6981(82)90271-2

12. Suellen C.S. Costa, A.., Lawrence L. Kazmerski. (2016). Dust and soiling issues and impacts relating to solar energy systems: Literature review update for 2012–2015. *Renewable and Sustainable Energy Reviews*, 33-61.
13. Tahboub, Z., Dahleh, B., & Goebel, O. (2011). *Solar Mirrors Soiling Campaign Abu Dhabi*. Paper presented at the Solar Power and Chemical Energy Systems (SolarPACES), Granada, Spain.
14. Wagner, F., Bortoli, D., Pereira, S., Costa, M. J., SILVA, A., Weinzierl, B.,. Heinold, B. (2009). Properties of dust aerosol particles transported to Portugal from the Sahara desert. *Tellus B, 61*(1), 297-306.
15. Wolfertstetter, F. (2013). *A Novel Method for Automatic Real-Time Monitoring of Mirror Soiling Rates.* Paper presented at the SolarPACES conference proceedings, Marrakech.
16. Wolfertstetter, F. (2016). Effects of Soiling on Concentrating Solarthermal Power Plants. Aachen: PhD thesis, University of Aachen.
17. Wolfertstetter, F., K. Pottler, N. Geuder, R. Affolter, A. A. Merrouni, A. Mezrhab, and R. Pitz-Paal. (2014). Monitoring of Mirror and Sensor Soiling with Tracs for Improved Quality of Ground Based Irradiance Measurements. *Energy Procedia*, 2422-2432.
18. Wolfertstetter, F., Wilbert, S., Fernández-García, A., & Azpitarte, I. (2018). Soiling and condensation model applied to a CSP solar field.
19. Wolfertstetter, F., Wilbert, S., Dersch, J., Dieckmann, S., Pitz-Paal, R., & Ghennioui, A. (2018). Integration of Soiling-Rate Measurements and Cleaning Strategies in Yield Analysis of Parabolic Trough Plants. *Journal of Solar Energy Engineering*, 140(144), 041008.